space applications, stainless steels higher in alloy than type 347 have not been used. Where higher strengths at elevated temperature are required, superalloys have been used, e.g., Inconel-N on the F-1 engine.

Conclusions

Brazed tube, regeneratively-cooled thrust chambers employing storable liquids (nitrogen tetroxide and Aerozine-50), seldom fail under classical burn-out conditions. Failure mechanisms observed are related to the actual deterioration of stainless steel tubing. Gas-metal reactions (i.e., carburization externally, and carburization and nitriding internally) occur that result in loss of ductility, metal loss on the exterior and interior of the tubes, and, finally, in structural failure (pinholes and cracking) of the weakened and thinned tube.

References

[1] Stanley, J. K., "The Carburization of Four Austenitic Stainless Steels," *ASTM Journal of Materials*, Vol. 5, No.4, 1970, pp. 957–971.

[2] Schley, J. R. and Bennett, F. W., "Destructive Accumulation of Nitrogen in 30Cr 20Ni Cast Furnace Tubes in Hydrocarbon Cracking Service at 1100°C," *Corrosion*, Vol. 23, No. 9, 1967, pp. 276–287.

[3] Stanley, J. K. and Perrotta, A. J., "Grain Growth in Austenitic Stainless Steels," *Metallography*, Vol. 2, 1969, pp. 349–362.

[4] Simon, F. F., Papell, S. S., and Simoneau, R. J., "Minimum Film-Boiling Heat Flux in Vertical Flow of Liquid Nitrogen," TN D-4307, 1968, NASA.

[5] Griffel, J., "Forced Connection Boiling Burn-Out for Water in Uniformly Heated Tubular Test Sections," NYO-187-7, May 25, 1965, U.S. Atomic Energy Commission.

[6] Stanley, J. K., "The Mechanical Properties of Carburized Austenitic Steels as Related to Microstructure," *Transactions of the International Conference on Quantitative Relation Between Properties and Microstructure*, Haifa, Israel, 1969.

[7] Stanley, J. K., "The Mechanical Properties of Nitrided Austenitic Steels as Related to Microstructure," *Transactions of the International Conference on Quantitative Relation Between Properties and Microstructure*, Haifa, Israel, 1969.

APRIL 1971 J. SPACECRAFT VOL. 8, NO. 4

Control Jet Interaction Investigation

BOB G. GILMAN*
Martin Marietta Corporation, Orlando, Fla.

An investigation of the interaction of control jets with the airstream surrounding a typical tactical missile configuration is reported. Rear-mounted bistable fluidic thrusters and circular sonic jets using air, nitrogen, and helium produced jet force amplification factors of about 1.6 to 2.2 at Mach numbers 0.9 to 2.0. Amplification factors near unity were measured at Mach 0.6. In general, amplification factors for a finned configuration were higher than for the model without fins.

Nomenclature

a_∞	= freestream speed of sound
A_J	= jet throat area
$C_N, \Delta C_N$	= normal force coefficient and increment from interaction
$C_{N\alpha 0}$	= normal force coefficient slope ($dC_N/d\alpha$) at $\alpha = 0$
D	= reference length (body diameter)
f	= fluid jet switching frequency
F_I, F_J	= interaction and jet forces
K	= jet interaction force amplification factor
M_J, M_∞	= jet exit and freestream Mach numbers
$\dot{m}_P$	= jet mass flow rate
P_e, P_J	= jet exit and jet chamber pressures
P_∞	= freestream static pressure
q_J, q_∞	= jet exit and freestream dynamic pressures
V_{exit}	= jet exit velocity
X_{cp}	= center of pressure
S	= reference area (body cross section)
α	= angle of attack
γ	= ratio of specific heats

Introduction

THE interaction between a control jet and the moving external airstream surrounding a missile can, under certain conditions, amplify the force of the control jet alone by a jet interaction (or amplification) factor K. Although numerous investigators have discussed jet interaction theory and test data at supersonic or hypersonic freestream conditions,[1–4] only limited data are available for subsonic or transonic conditions. Reference 5 discusses effects of jet gas molecular weight and jet exit Mach number M_J on amplification factor and jet penetration and correlates test data with Dahm's[6] theoretical prediction. Cassel[7] reports amplification factors of 0.5 to 0.9 for forward located jets at subsonic conditions. Kuiper[8] presents data for steady-state jets similar in shape to those reported herein which show the same amplification trends. However, his values of K never go below 1 subsonically and peak near 2 at $M_\infty = 1.0$, whereas the present data peak at about $K = 2.3$ near $M_\infty = 1.2$.

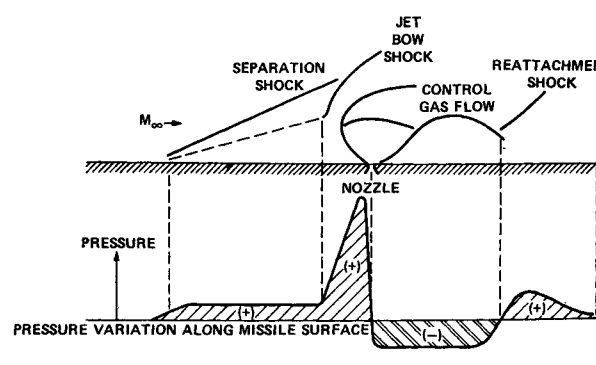

Fig. 1 Jet interaction phenomenon.

Received November 16, 1970; revision received January 18, 1971.

* Staff Engineer, Aerophysics Department. Associate Fellow AIAA.

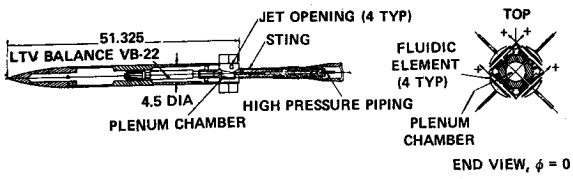

Fig. 2 Model assembly.

Amplification occurs when the force due to positive surface pressure (usually found in front of the reaction jet) is greater than the force in the opposite direction caused by lower surface pressure (behind the jet). Figure 1 depicts this phenomenon at supersonic speeds. The objective of this research was to obtain K's for a typical tactical missile in transonic and low supersonic flight. Of particular interest was the use of bistable fluidic diverters for control jets and the effect of thrust modulation and oscillating frequency on the resulting K's. A single, circular, sonic jet was also tested under steady-state conditions for comparison purposes. A wind-tunnel test program was conducted in the Ling-Temco-Vought High Speed Wind Tunnel described in Ref. 9. The K's were obtained by comparing model aerodynamic forces and moments measured on a strain gage balance with and without jet flow.

Experimental Setup

Figure 2 shows the model and mounting sting. The control jet systems are located $\sim\frac{1}{3}$ body diameter ahead of the model base. For this test program the model and balance roll together (except for the sonic jet configuration) and the normal force coefficient (C_N) is always in the pitch plane. The fluidic elements which provide the jet flow are mounted on the plenum chamber-sting and their thrust is not carried on the balance. This jet thrust was determined in a separate calibration prior to the wind-tunnel test. Four fluidic diverters are operated in pairs on the opposite sides of the model to provide the desired control force. For the oscillating runs each element is continually switched from one side to the other (+ to −). When no control is needed, each side operates 50% of the time; when control is needed, one side stays on longer than the other. Figure 3 shows the diverter cross section with two typical M_J distributions.

The balance selected for this program had a high moment-carrying capability and extremely small angular deflections in the pitch and yaw planes under load. If was important to keep the angular deflections small because of the small clearance between the jets mounted on the sting and the model shell mounted on the balance. This type of model design was necessary for dynamic operation of the fluidic diverters and good simulation of the control jet operation.

A schematic drawing of the equipment needed to operate and control the two types of reaction jets used in this program is shown in Fig. 4. The valves, gas supply bottles, and flow meter in the top portion of the drawing were used primarily to supply injectant gas to the reaction jet systems. The oscilloscopes, RPM control, and flow regulators at the bottom were used to control the switching of the fluidic diverters only. The cam and motor shown in the center part were used to switch and modulate the fluidic jets. The fluidic diverters, transducers, and balance in the center part were used to obtain primary test data and were located inside the model shell.

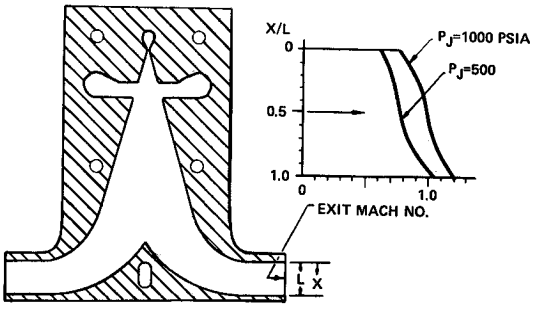

Fig. 3 Fluidic element and exit Mach numbers.

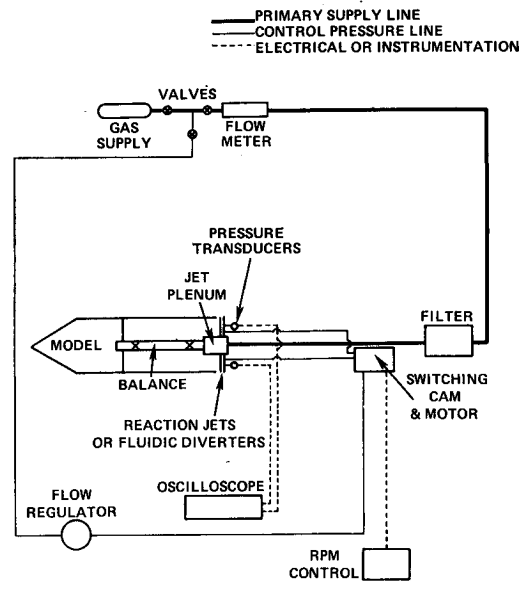

Fig. 4 Jet control schematic.

Jet Performance

The fluidic system tested in this investigation was designed for tactical missile applications. A full-scale control system would include a two-axis fluidic gyro with fluidic logic feeding bistable fluidic diverter reaction jets. The advantages of such a system are simplicity, reliability, few moving parts, and the ability to produce the rapid response and control forces required for tactical missiles. In this test, the two-axis gyro was replaced by a motor and cam system to control thrust modulation and switching frequency. The fluidic reaction control jets were reduced in size and thrust capability in keeping with the model dimensions and wind tunnel conditions.

For the missile configuration under investigation each full-scale fluidic jet was designed to produce 50 lb of thrust and switch at a frequency of 50 Hz. To simulate the performance of these units in the wind tunnel two scaling parameters were used. The following relationship was used to size the thrust of the fluidic jets.

$$[F_J/q_\infty S]_{\text{full scale}} = [F_J/q_\infty S]_{\text{wind tunnel}} \quad (1)$$

Since the model is smaller than full scale and the speed of

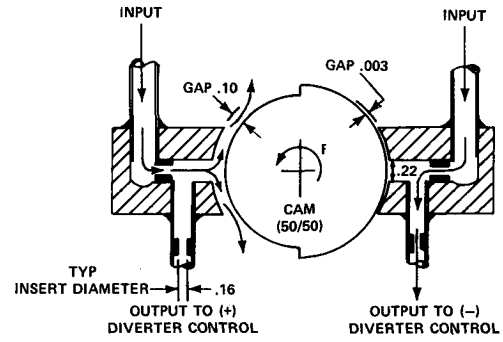

Fig. 5 Diverter switching control schematic.

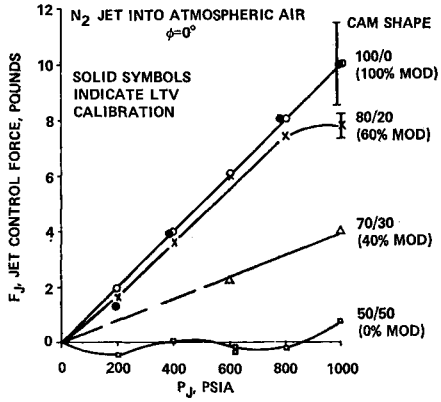

Fig. 6 Variation of fluidic jet control force with chamber pressure for several cam shapes.

sound in the wind tunnel is different, the switching frequency was scaled according to

$$[fD/a_\infty]_{\text{full scale}} = [fD/a_\infty]_{\text{wind tunnel}} \quad (2)$$

The cam system sketched in Fig. 5 was used to vary thrust modulation and switching frequency. The duration of the control flow to the (+) and (−) sides of the fluidic diverters was determined by the cam shape. When the cam gap was small (0.003 in.), the flow went to the diverter; when the gap was large (0.1 in.), the flow was vented before it reached the diverter. The secondary mass flow needed for switching the fluidic jets was about 15 to 20% of the primary flow, depending on operating conditions. The rotational speed of the cam system determined the switching frequency. Opposing diverters were coupled together to avoid induced rolling moments.

The jet control force from four fluidic diverters, mounted on the sting at $\Phi = 0°$ and flowing as shown in Fig. 2, was determined in calibration tests on a thrust stand which was previously calibrated by applying a known force at the jet exit location and measuring the deflection of the spring-loaded arm. The estimated overall accuracy of the calibrated stand was 10%. Care was taken to position the fluidic jet supply lines such that all gas-flow momentum contributions were cancelled. Data were taken over a backpressure range of 4.4 to 19.7 psia for model roll positions of 0 and 45°.

Other force data at the facility were obtained from a strain gage mounted on the sting system. Data were taken for various control cam shapes corresponding to a desired range of force modulation factors at several switching frequencies. Variation of the control force F_J with chamber pressure and cam shape for atmospheric backpressure is shown in Fig. 6.

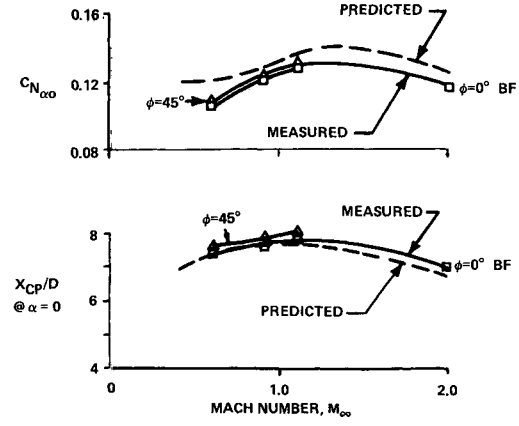

Fig. 7 Variation of normal force coefficient slope and center of pressure with Mach number.

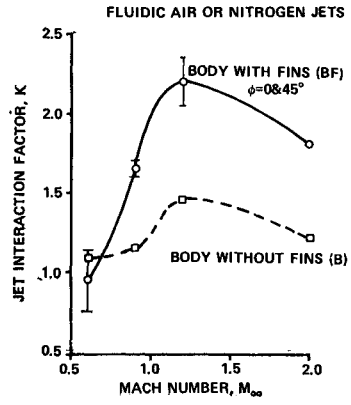

Fig. 8 Variation of jet interaction factor with Mach number for scaled thrust conditions.

The control forces obtained from the calibration stand were used in the subsequent calculation of fluidic jet interaction amplification factors for all altitudes and Mach numbers tested. Sonic jet control forces were calculated using the following equation for all injectant gases:

$$F_J = [P_e(\gamma_J M_J^2 + 1) - P_\infty]A_J \quad (3)$$

Test Results

The primary data source was a 5-component strain gage balance with which model normal force, pitching moment, side force, yawing moment, and axial force were measured. This balance did not measure any reaction jet control force because the jets were mounted on the sting system behind the balance. Model surface, base, and cavity pressures as well as those pressures necessary to determine the performance of the reaction jets were also measured. For most of the runs shadowgraphs of the jet interaction flow field were taken. For specified runs, oil-flow photographs of the flow on the model surface near the jet openings were also made.

The average freestream test conditions for all the test runs are shown in Table 1. Run-to-run variations in freestream properties did not deviate from the values shown here by more than 1 or 2%. All runs were made with an α range of at least ±6°; several went to ±10°.

For the jet-off case, the variation of $C_{N\alpha 0}$ and X_{cp}/D with M_∞ are shown in Fig. 7 for the basic configuration BF at roll angles of 0° and 45°. There is very little change in the data with roll angle. Experimental values agree with predicted values within ~10% for $C_{N_{\alpha 0}}$ and 5% for X_{cp}. The jet interaction amplification factor is defined as

$$K = (F_J + F_I)/F_J = 1 + F_I/F_J \quad (4)$$

where F_J is obtained from the previously discussed calibration for the fluidic jets and from Eq. (3) for the sonic jet. The jet interaction normal force F_I is defined as

$$F_I = \Delta C_N q_\infty S \quad (5)$$

where ΔC_N is the change in C_N due to the addition of jet interaction.

The flow through the small opening in the body through which the jet flow emerges has been estimated from the measured pressure differential across the opening. Maximum force due to this flow for the scaled trajectory conditions is

Table 1 Average freestream test conditions

M_∞	q_∞, psi	p_∞, psia	R_N/ft	T_0, °R
0.6	4.8	19.3	5.5×10^6	572
0.9	9.7	17.1	8.0×10^6	587
1.1	9.7	11.6	7.2×10^6	590
2	12.5	4.4	8.7×10^6	563

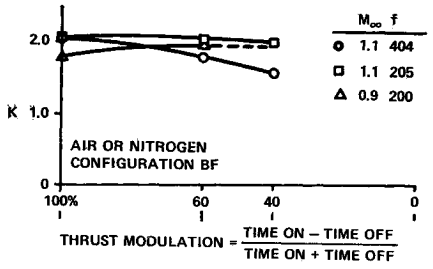

Fig. 9 Variation of jet interaction factor with modulation.

about 10–12% of the jet interaction forces measured. Variation of cavity pressure just inside the opening from the jet off to jet on condition was less than the data scatter of ~4%.

Amplification Factor

Figure 8 shows $K = f(M_\infty)$ for steady-state (nonswitching) scaled trajectory conditions for configurations BF and B (without fins). At $M_\infty = 0.6$, $K \cong 1$ for both configurations. ($K < 1$ would indicate a loss of reaction jet force.) At the higher M_∞'s the finned configuration produces K's from 1.8 to 2.2, while the maximum K for the configuration without fins is about 1.5. Apparently, the fins confine the jet interaction flow field and increase amplification.

The variation of K with thrust modulation (for cam shape) is shown in Fig. 9 for configuration BF at scaled trajectory conditions. For the conditions tested, K does not appear to be significantly affected by thrust modulation. Some of the data scatter in this figure is attributed to the erratic switching behavior of the fluidic diverters which was experienced at times and which is attributed to the inability of the cam system to produce good square waves at some of the higher frequencies and short durations. The flight configuration with complete fluidic controls would not suffer from this problem. Data for the zero modulation case are not shown because of the large scatter in them. This is to be expected since K is a function of F_I/F_J and both of these quantities approach zero for zero thrust modulation.

The local jet interaction flow and boundary-layer behavior appear to follow the jet switching frequency for all frequencies tested, as seen from Fig. 10, where P_{E4} is the pressure measured just inside the fluidic nozzle exit on the positive side of diverter 4, and P_{G1} and P_{L3} are pressures measured just ahead of the number 4 jet opening. Both of the latter pressures follow the jet outflow closely. The apparent lag of about 1.3 msec between P_{E4} and P_{L3} corresponds closely to the time required for a pulse to travel from the pressure orifice through one foot of tubing to the sensing element at the local speed of sound. This indicates that the flow at the orifice has almost instantaneous response to the jet outflow behind it.

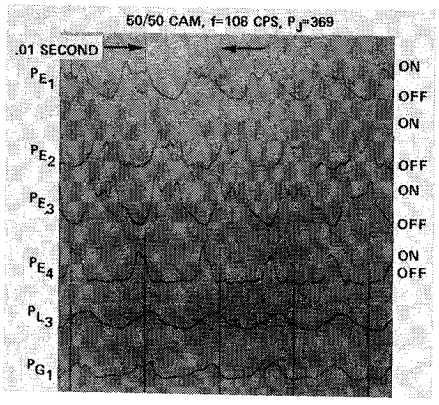

Fig. 10 Oscillograph pressure traces.

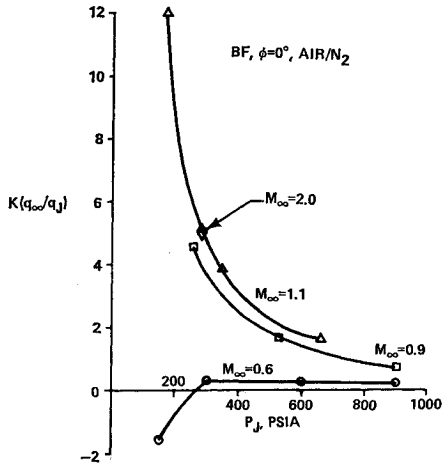

Fig. 11 Variation of K (q_∞/q_J) with jet chamber pressure.

Figure 11 shows Kq_∞/q_J vs P_J for several M_∞'s. The dynamic pressure ratio (q_∞/q_J) is equivalent to the momentum ratio of the two impinging flows and should be a good relationship for correlating jet interaction phenomena for various flow conditions. This correlation appears to work fairly well for all conditions except the subsonic Mach number, which might be expected since the flow pattern produced by the strong bow shock is not present here. In general, the rapid decrease of Kq_∞/q_J with increasing P_J is due to an increase in F_J, rather than a decrease in F_I, since $K \to 1$ as F_J increases and F_I remains constant by the earlier definition.

For comparison, a single circular sonic jet was run in the steady-state mode at $M_\infty = 2.0$. The throat of this sonic jet was sized to produce the same F_J as the fluidic system at ambient quiescent conditions and $P_J = 1000$ psia. The gases used for each system were air (or nitrogen) and helium. It was felt that the lower molecular weight and higher speed of

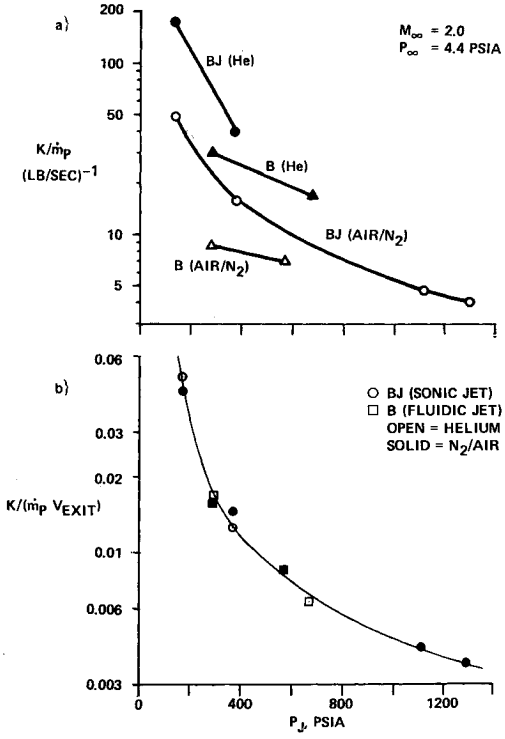

Fig. 12 Variation of $K/\dot{m}_P$ and $K/(\dot{m}_P \times V_{exit})$ with chamber pressure.

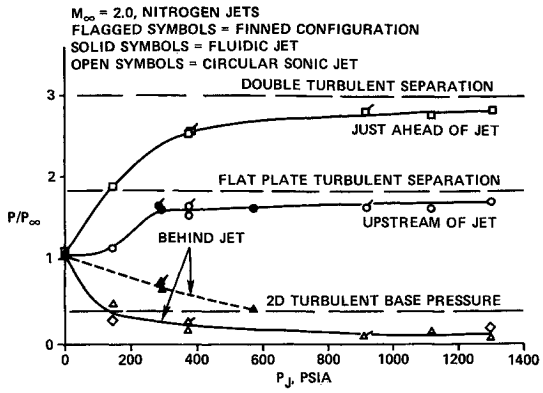

Fig. 13 Surface pressure comparison.

sound for helium would more nearly simulate the hot gas jet behavior. Since K is also affected by mass flow variations, for purposes of comparison, $K/\dot{m}_p$ was plotted vs P_J in Fig. 12a. From this comparison it can be concluded that the single sonic jet has an amplification factor 30 to 40% higher than the four-diverter fluidic jet system for the same mass flow. Furthermore, K's for helium are about twice as large as those for air or nitrogen for both jet systems.

If the same data are compared on a momentum basis by dividing $K/\dot{m}_p$ by the average exit velocity of each gas and jet, the correlation shown in Fig. 12b results. From this it would appear that both jets and all gases produce the same amplification when compared on a momentum basis at the same chamber pressure.

Figure 13 shows that at high P_J's, the surface pressure ratio P/P_∞ just ahead of the jet approaches the theoretical value for double turbulent separation suggested as an upper limit criterion in Ref. 4. The pressure further upstream (about 5 jet diameters) approaches the level produced by turbulent separation on a flat plate and is about the same for both the fluidic and the sonic jets. However, the behavior of the pressure behind different jets is different. The pressure ratio behind the sonic jet is much lower. This difference in behavior behind the jets may also be seen in the oil flow photographs of Fig. 14.

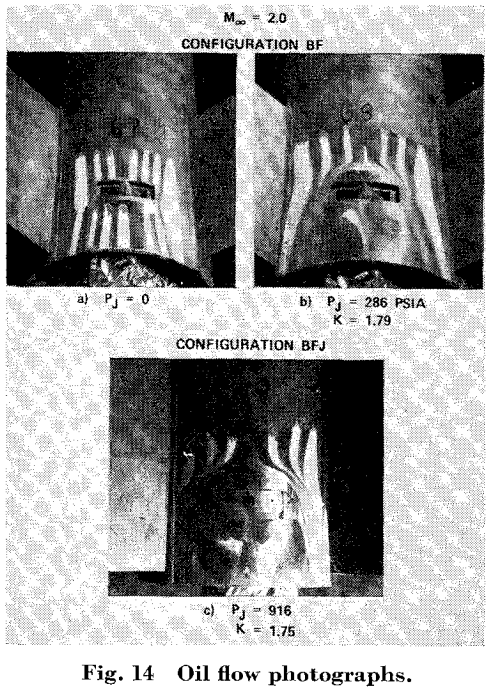

Fig. 14 Oil flow photographs.

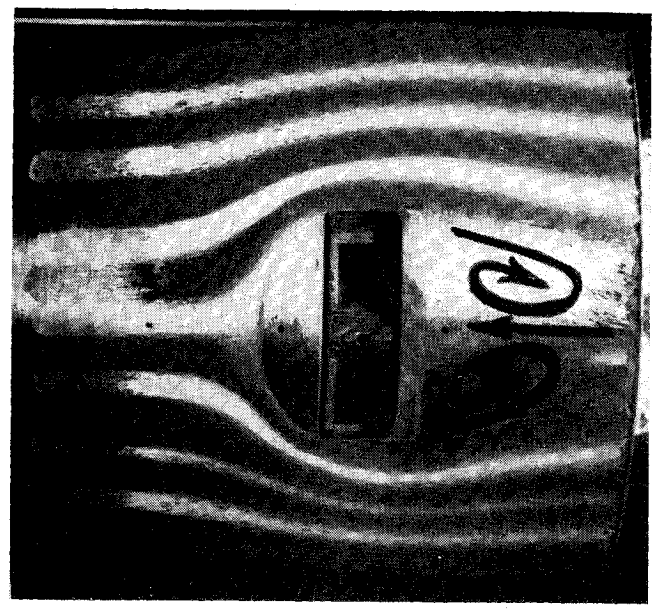

Fig. 15 Oil flow photograph.

Oil Flow Photographs

Small drops of oil paint in alternating colors were put on the model ahead of the area under investigation. During the run this oil flowed in the direction of the surface flow streamlines, leaving a pattern which was photographed after the run. Areas where the two colors have mixed or where there is no color indicate highly turbulent or separated flow.

The flow pattern for the finned configuration with jets off is shown in Fig. 14a. The compression and expansion flow around the fins is well defined and there is no indication of separated flow anywhere on the body. Figure 14b shows the scaled trajectory condition with the rectangular fluidic jets on. The positive pressure area in the separated region ahead of the jet is quite obvious. An oil-flow photograph of the flow around the sonic jet is presented in Fig. 14c. A similar separated flow area ahead of the jet can be seen. However, the wake behind the sonic jet is divergent, while behind the fluidic jet it is more nearly convergent moving rearward.

Better flow detail can be seen in Fig. 15. The base flow here very much resembles the classical two-dimensional base flow pattern which has a pair of trapped vortices with upstream flow between them. The level of the pressure ratio behind the fluidic jet also indicates this type of flow, since it agrees closely with that predicted for two-dimensional turbulent base pressure (Fig. 13).

Photographs 14b and 14c also show that the jet interaction flow is being confined between the fins and may even be impinging on the fin roots. This behavior could explain the increased K measured on the finned configuration.

Conclusions

Jet interaction amplification factors greater than unity were experienced for all configurations and reaction jet systems tested at freestream Mach numbers of 0.9 and above. At $M_\infty = 0.6$ the factor for configuration BF was near or slightly below unity.

The finned configuration generally produced amplification factors 30 to 40% higher than the body without fins at supersonic speeds. The thrust-modulated, oscillating fluidic jet system performed reasonably well except for some erratic and uncertain switching behavior at the high frequencies and short pulse durations due to the control cam system. For all conditions tested the interaction flow ahead of the jet followed the jet pulses with no apparent lag.

For the same jet chamber pressure at Mach 2.0, the single, sonic jet produced higher amplification factors per pound of mass injected than the four-diverter fluidic jet system. Jet interaction amplification factors were also larger per pound of gas injected for helium than they were for air or nitrogen at the same chamber pressure for the conditions tested. However, both jets and all gases produced the same amplification when compared on a momentum basis.

The flow pattern and pressure behind the fluidic jet very much resembled the classical two-dimensional base flow phenomenon.

References

[1] Spaid, F. W., Zukoski, E. E., and Rosen, R., "A Study of Secondary Injection of Gases Into a Supersonic Flow," TR 32-834, Aug. 1966, Jet Propulsion Lab., California Institute of Technology, Pasadena, Calif.

[2] Cassel, L. A., Davis, J. G., and Engh, D. P., "Lateral Jet Control Effectiveness Prediction for Axisysmmetric Missile Configurations," Rept. RD-TR-68-5, June 1968, U. S. Army Missile Command, Redstone Arsenal, Ala.

[3] Kaufman, L. G., "Interaction Between High Speed Flows and Transverse Jets: A Method for Predicting the Resultant Surface Pressure Distribution," Rept. RE-348A, April 1969, Grumman Aircraft Engineering Corp., Bethpage, N. Y.

[4] Werle, M. J., "A Critical Review of Analytical Methods for Estimating Control Forces Produced by Secondary Injection," NOLTR 68-5, Jan. 1968, U. S. Naval Ordnance Lab., White Oak, Md.

[5] Koch, L. S. and Collins, D. J., "The Effect of Varying Secondary Mach Number and Injection Angle on Secondary Gaseous Injection Into a Supersonic Stream," AIAA Paper 70-552, Tullahoma, Tenn., 1970.

[6] Dahm, T. J., "The Development of an Analogy to Blast Wave Theory for the Prediction of Interaction Forces Associated with Gaseous Secondary Injection into a Supersonic Stream," TN 9166-TN-3, May 1964, Vidya Corp., Palo Alto, Calif.

[7] Cassel, L. A. et al., "Jet Interaction Control Effectiveness for Subsonic and Supersonic Flight," Rept. RD-TR-69-21, Sept. 1969, U. S. Army Missile Command, Redstone, Arsenal, Ala.

[8] Kupier, R. A., "Control Jet Effectiveness in the Subsonic and Transonic Regimes," Rept. U-2932, Dec. 1964, Philco Aeronautic Div. of the Ford Motor Co., Newport Beach, Calif.

[9] Wolfe, J. A., "High Speed Wind Tunnel Handbook," LTV Publication AFR-EIR-13552-A, June 1968, LTV Aerospace Corp., Dallas, Texas.

APRIL 1971 J. SPACECRAFT VOL. 8, NO. 4

Thermal Radiation Absorption by Particle-Seeded Gases

J. R. Williams,* W. L. Partain,† A. S. Shenoy,‡ and J. D. Clement§
School of Nuclear Engineering, Georgia Institute of Technology, Atlanta, Ga.

Particle-seeded gases are currently being considered as propellants for gas core nuclear rocket engines and for other applications such as thermal shielding for re-entry vehicles and rocket nozzle cooling which require that surfaces be protected from intense thermal radiation. To evaluate radiant heat transfer through a particle-seeded gas, one must know the extinction parameter, the scattering parameter, and the scattering amplitude function of the particles. The extinction parameters of submicron particles dispersed in hydrogen at 1 atm pressure have been measured as a function of wavelength from 1200 to 6800 Å at various temperatures to 2170°K and are ~50,000 cm²/g for carbon, ~20,000 cm²/g for tungsten, and ~65,000 cm²/g for silicon. The extinction parameter of submicron tungsten particles in hydrogen at 12.5 atm showed an increase to ~50,000 cm²/g as the temperature was raised to 2030°K, and at 100 atm it reached ~100,000 cm²/g at 2300°K. The scattering amplitude functions of submicron carbon, tungsten, silicon, tungsten carbide, and silicon carbide dispersed in nitrogen were measured and scattering from these particles was shown to be highly forward, that is, most of the scattered light is scattered at angles <30°.

Nomenclature

I = intensity of a beam of radiant energy
j = emission coefficient
k = linear attentuation coefficient
p = scattering amplitude function
s = distance variable
x = path length through a particle cloud
θ = angle of scattering
λ = wavelength
μ_a = absorption parameter
μ_e = extinction parameter
μ_s = scattering parameter
ρ = mass of particles per unit volume of aerosol
Ω,Ω' = solid sngles

Received February 6, 1970; presented as Paper 70-838 at the AIAA 5th Thermophysics Conference, Los Angeles, Calif., June 29–July 1, 1970; revision received December 14, 1970. The research described in this paper was supported by NASA grant NGR-11-002-068 and administered by the Nuclear Systems Division of the NASA Lewis Research Center. The authors would like to thank W. R. Jacobs, an AEC Fellow in the School of Nuclear Engineering, for his work on the scattering measurements. The authors especially appreciate the many helpful suggestions given them by C. Masser of the Nuclear Systems Division of the NASA Lewis Research Center.

* Assistant Professor. Member AIAA.
† Research Assistant.
‡ Research Engineer; presently with the Gulf General Atomic Corp.
§ Professor.

Introduction

THE absorption of thermal radiation by a gas is usually greatly enhanced by the dispersion of small metallic particles in the gas. The particles absorb radiant energy and